Simultaneous imaging of vibrational, rotational, and electronic wave-packet dynamics in a triatomic molecule

Huynh Van Sa Lam [1,*] Van-Hung Hoang [1] Anbu Selvam Venkatachalam [1] Surjendu Bhattacharyya [1]
Keyu Chen [1] Sina Jacob [2] Sanduni Kudagama [1] Tu Thanh Nguyen [1] Daniel Rolles [1] Uwe Thumm [1,†]
Artem Rudenko [1,‡] and Vinod Kumarappan [1,§]

[1] *James R. Macdonald Laboratory, Kansas State University, Manhattan, Kansas 66506, USA*
[2] *Institut für Kernphysik, Goethe-Universität Frankfurt, 60438 Frankfurt am Main, Germany*

Light-induced molecular dynamics often involve the excitation of several electronic, vibrational, and rotational states. Since the ensuing electronic and nuclear motion determines the pathways and outcomes of photoinduced reactions, our ability to monitor and understand these dynamics is crucial for molecular physics, physical chemistry, and photobiology. However, characterizing this complex motion represents a significant challenge when different degrees of freedom are strongly coupled. In this Letter, we demonstrate how the interplay between vibrational, rotational, and electronic degrees of freedom governs the evolution of molecular wave packets in the low-lying states of strong-field-ionized sulfur dioxide. Using time-resolved Coulomb explosion imaging (CEI) and quantum mechanical wave packet simulations, we directly map the bending vibrations of the molecule, show how the vibrational wave packet is influenced by molecular alignment, and elucidate the consequences of nuclear motion for the coupling between the two lowest electronic states of the cation. Our results demonstrate that multicoincident CEI can be an efficient experimental tool for characterizing coupled electronic and nuclear motion in polyatomic molecules.

Recording molecular movies—tracking the motion of individual atoms during ultrafast structural changes with sufficient spatiotemporal resolution—has been a longstanding goal in molecular optical sciences [1–4]. Remarkable progress toward this goal has been demonstrated recently, largely driven by the development of gas-phase ultrafast electron diffraction (UED) [5,6] and ultrafast x-ray scattering (UXS) [7–9], which are particularly sensitive to nuclear motion. Together with spectroscopic methods sensitive to the electronic structure and advanced theoretical modeling, these techniques have provided critical insights into several important photochemical reactions [2,6,10]. However, despite the variety of available experimental tools, complete and unambiguous characterization of molecular dynamics remains challenging. Central to these challenges is the ubiquitous interplay between nuclear and electronic motion, which underpins essential processes in photochemistry, photophysics, and photobiology, including energy transfer, photodissociation, and nonradiative relaxation [11]. Such coupled motions are inherently complex, even for small polyatomic molecules [12]. Electronic excitations reshape molecular geometries and populate a variety of vibronic levels, while nuclear-electronic couplings enable nonadiabatic transitions near conical intersections, where electronic states converge [13].

Time-resolved Coulomb explosion imaging (CEI) is another method used to create molecular movies [14–20]. While CEI does not directly yield real-space molecular geometries, it provides excellent temporal resolution, high sensitivity to light atoms, and accessibility in university-scale laboratories. Critically, unlike UED and UXS, which project structural information onto a single coordinate (momentum transfer), coincidence-mode CEI [21–27] generates high-dimensional data with naturally embedded correlations that enable reliable separation of reaction pathways, even for rare stochastic processes [28]. Previously, both CEI and diffraction-based techniques have been employed to directly image light-induced rotational [15,19,29–31] and vibrational [8,23, 32–34] wave packets, which play a critical role in many types of molecular dynamics [35–43]. However, most experimental movies of molecular vibrations have been limited to diatomic molecules (such as H_2^+ [23,44], D_2^+ [45,46], N_2^+ [47], O_2^+ [47,48], CO^+ [47,49], and I_2 [32–34]) or the stretching of just one bond in polyatomic molecules [50–52]. Due to the fast time scale and complexity of rovibronic motions in polyatomic molecules, only a limited number of direct structural measurements of other vibrational modes has been reported [8,53,54].

In this Letter, we demonstrate that laser-induced Coulomb explosion can directly image ultrafast coherent wave packets in a small polyatomic molecule and produce movies that show the motion of individual atoms even in the presence of coupled nuclear and electronic motion. We investigate sulfur dioxide (SO_2), a bent triatomic molecule that has been studied extensively (see, for instance, Refs. [16,22,55–63]) due to its significance in atmospheric processes and its intriguing

*Contact author: huynhlam@ksu.edu
†Contact author: thumm@ksu.edu
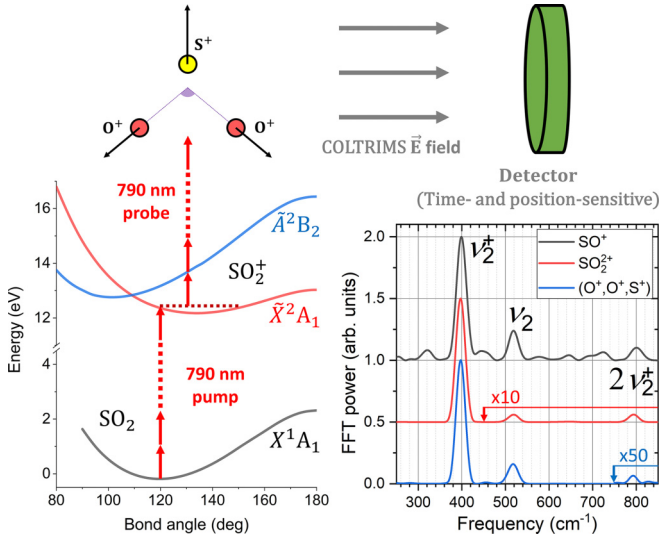‡Contact author: rudenko@ksu.edu
§Contact author: kumarappan@ksu.edu

FIG. 1. Pump-probe scheme and relevant potential energy curves. The bottom-right inset shows FFT spectra of the delay-dependent yield of SO^+, SO_2^{2+}, and the three-body (O^+, O^+, S^+) channel. For the three-body channel, only events that have the angle between two O^+ momentum vectors from $80°$–$115°$ were selected.

photochemistry, including the efficient formation of neutral and ionic molecular oxygen [64–67]. We employ time-resolved coincident CEI to create a movie of the coherent vibrational wave packet in SO_2^+ and show that its dynamics are significantly influenced by the rotational motion. Moreover, we find that a secondary wave packet resulting from a resonant dipole coupling between the two lowest electronic states of SO_2^+ traverses a conical intersection and leaves clear signatures of the nonadiabatic coupling between these two states in the ion momentum distributions.

Our experiment utilized a Ti:Sapphire laser operating at 10 kHz, generating near-infrared (NIR) pulses with a central wavelength of approximately 790 nm and a pulse duration of about 28 fs. We split this output into pump and probe pulses, with independently controlled power, and scan their relative delay using a motorized linear stage. As depicted in Fig. 1, we use a 3.4×10^{14} W/cm^2 pump pulse to ionize SO_2 and a 8×10^{14} W/cm^2 probe pulse to further ionize and dissociate (i.e., Coulomb explode) it. The ions are then detected in coincidence using a COLTRIMS apparatus [68]. The momenta of these ions, determined from their measured time of flight and impact position, are used to deduce information about the induced wave packets.

Previous studies [69–72] have reported that the bending mode progression dominates the SO_2^+ ($\tilde{X}^2A_1$)←SO_2 (X^1A_1) photoelectron spectra because the equilibrium geometries in these electronic ground states have almost identical bond lengths but different bond angles [69,73]. This leads to a strong excitation into the bending mode (ν_2^+) and very weak excitation into the symmetric (ν_1^+) and asymmetric (ν_3^+) stretch modes. The first seven bending-mode energies are approximately equally spaced with a nearest-neighbor separation of ≈ 400 cm^{-1}. In our experiment, which has a 17 cm^{-1} frequency resolution, we see oscillations at this frequency (and its first overtone at ≈ 800 cm^{-1}) in different

observables for various ionization and fragmentation channels. This indicates that these channels involve the population of the SO_2^+ ground state by the pump pulse and subsequent ionization and/or fragmentation by the probe. For example, the fast Fourier transform (FFT) spectra of the delay-dependent yields of SO^+, SO_2^{2+}, and (O^+, O^+, S^+) channels show a strong peak at the bending frequency and a much smaller one at the overtone (Fig. 1). They also show a weak but clear signature of the bending vibration in the ground state of neutral SO_2 (at 520 cm^{-1}) [74]. The latter could be induced by Raman excitation (analogous to bond softening), or by geometry-dependent ionization (so-called Lochfrass process) [45,51,75–77]. The determination of the relative importance of these mechanisms requires a detailed analysis of the wave packet phase and will be discussed elsewhere. Here, we focus on the three-body channel to directly visualize the bending vibrations of the cation via delay-dependent kinetic energy (KE) spectra and angle correlations between the fragment ions.

In Fig. 2, we present experimental data from the (O^+, O^+, S^+) channel illustrating the delay dependence of several key observables: [Fig. 2(a)] the angle between the momentum vectors of two O^+ ions [$\angle(O^+, O^+)$], [Fig. 2(b)] the KE of S^+ fragment [KE(S^+)], and [Fig. 2(c)] the total KE of two O^+ fragments [KEsum(O^+, O^+)]. Simulation results are depicted in Figs. 2(d)–2(f). The delay-dependent mean values of experimental data in Figs. 2(a)–2(c) are shown in Fig. 2(g). Figure 2(h) features distributions of the ions at 250 fs (scatter plot) and 210 fs (contour line) when the bending wave packet is at the inner and outer turning points, respectively.

There are two distinguished features in the experimental data shown in Figs. 2(a)–2(c). First, all observables—$\angle(O^+, O^+)$, KE(S^+), and KEsum(O^+, O^+)—show pronounced oscillations with a period of 83 fs (or 400 cm^{-1}), clearly indicating that we mainly image the vibrational wave packet in the ground state of SO_2^+ [70]. Second, there is a clear correlation between these observables: $\angle(O^+, O^+)$ and KEsum(O^+, O^+) oscillate in-phase with each other and out-of-phase with KE(S^+). This can be explained in terms of Coulomb forces between point charges (see Fig. S3 in the SM [78]): near the equilibrium geometry, the net force on the S^+ (O^+) fragment due to the other two decreases (increases) with increasing bond angle. Moreover, $\angle(O^+, O^+)$ also increases monotonically with the real-space bond angle.

We numerically model the experimental observables in Figs. 2(a)–2(c) by solving the time-dependent Schrödinger equation for the coupled nuclear motion on the Born-Oppenheimer potential energy surfaces (BOS) of the $SO_2(X)$ and $SO_2^+(\tilde{X})$ states, including all vibrational degrees of freedom (symmetric stretch, bending, and antisymmetric stretch modes) [85]. We calculate the BOS *ab initio* by applying the multiconfigurational self-consistent-field method as implemented in the quantum chemistry code GAMESS [86], based on seven frozen inner orbitals and 12 active orbitals expanded in the correlation consistent-polarized valence triple-zeta (cc-pVTZ) basis set. We account for single ionization of $SO_2(X)$ to $SO_2^+(\tilde{X})$ by propagating the nuclear wave functions of the neutral and cationic states subject to dipole coupling by the pump pulse, with the assumption that the photoelectron has zero kinetic energy [85]. Within this *ad hoc* dipole-coupling
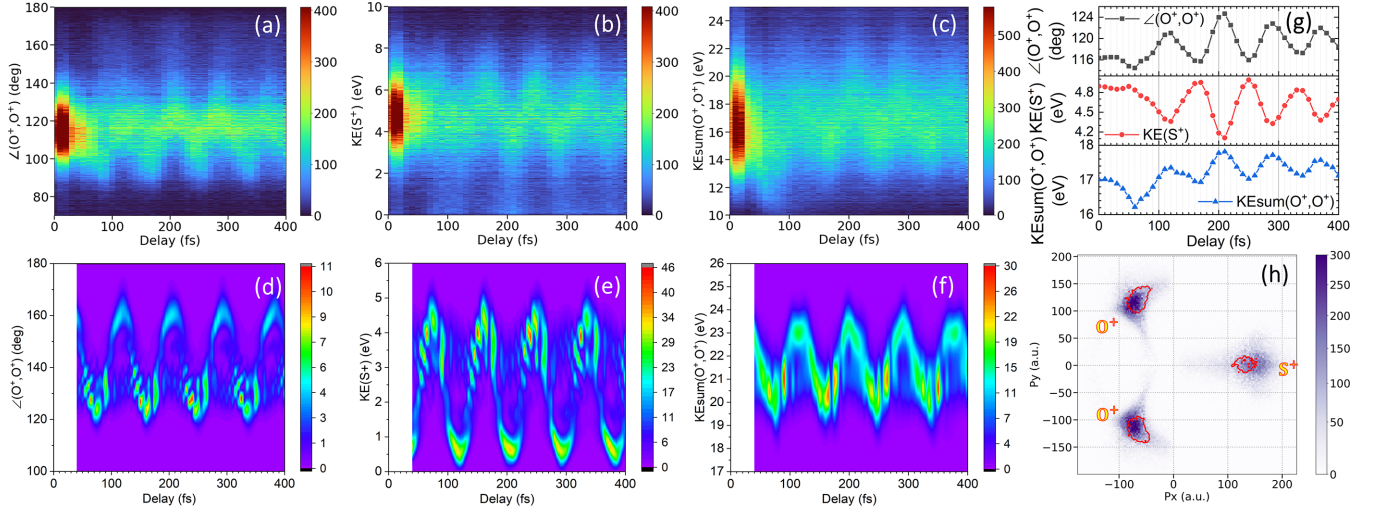
FIG. 2. Signatures of bending vibrations in $SO_2^+(\tilde{X})$: Measured delay dependence of (a) angle between the two O^+ momenta, (b) KE of S^+, and (c) total KE of the two O^+ fragments. (d)–(f) show simulations of the observables in (a)–(c); note the different vertical scales for each pair. (g) presents the mean of experimental observables in (a)–(c) as a function of pump-probe delay. (h) shows the Newton plot at 250 fs when the bending wave packet reaches the inner turning point. The red contour (at 1/3 maximum intensity) represents the distribution at 210 fs when the bending wave packet reaches the outer turning point. The x axis is defined as the bisector between the two O^+ momenta, and the vector difference between them defines the xy plane [79]. A timed sequence of these images illustrating the motion of individual atoms is provided in the Supplemental Material (SM) [78], which includes Refs. [80–84]. In all two-dimensional (2D) plots, the color bar indicates the yield. To emphasize the pump-induced effects, we subtracted the probe-only contributions in (a)–(c) and (h). No subtraction was used in subsequent analyses, and the original data is provided in Fig. S1 of the SM. We discarded events with KER < 14 eV to remove dissociating molecules.

model, the neutral ground state is depleted (and the ionic state populated) throughout the pulse, resulting in coherent vibrational wave packets in both states [45,75]. To account for multiple ionization in the delayed probe pulse, we project the SO_2 and SO_2^+ nuclear wave functions onto the potential energy surface of the triply charged molecule, approximated as purely Coulombic. We then propagate the ensuing nuclear wave packet representing the S^+ and the two O^+ ions to sufficiently large internuclear distances to reach numerical convergence of their momentum expectation values. We obtain the fragment KEs by FFT of the real-space nuclear wave function to momentum space [87].

Our simulations shown in Figs. 2(d)–2(f) closely resemble the experimental data in Figs. 2(a)–2(c), manifesting similar periodicity, phases, and correlations between the three observables. However, each pair of experiment-simulation plots shows a mismatch in absolute values of angle or KE. The primary reason for this mismatch is that vertical projection to and propagation on the Coulomb potential, which we used in our simulation, do not accurately describe the ionization and fragmentation process caused by the probe pulse. Furthermore, as will be discussed below, the wave packet propagation on the $\tilde{A}^2 B_2$ state, which extends to smaller bond angles and is not included in our simulation, also contributes to the experimental data (see also Fig. S3 in the SM [78]). Nevertheless, our results provide a direct intuitive picture of the strong-field-induced vibrational wave packet motion in a triatomic molecule. Modulations of this three-body channel are dominated by the ionic ground-state vibrations, with a weak contribution from bending vibrations in the ground state of neutral SO_2, as revealed by FFT of the delay-dependent data (Fig. 1 and SM, Fig. S2 [78]).

Besides revealing the states involved in the vibrational wave packet, coincidence momentum imaging also allows us to visualize the correlated motion of individual atoms. To achieve this, we plot the data for all ions from the (O^+, O^+, S^+) channel in a 2D momentum image (Newton plot). Figure 2(h) features a representative image at 250 fs with a contour for data at 210 fs (the inner and outer turning points of the bending wave packet). Because the $\angle(O^+, O^+)$ and $KE(S^+)$ manifest the same behavior as the OSO bond angle and the displacement of S from the center of mass (Fig. 2 and Fig. S3 [78]), movies comprising a timed sequence of these images (as provided in the SM [78]) are a striking and intuitive representation of the bending vibration of the molecule. These molecular movies illustrate that during the first 400 fs, the wave packet is well localized and mimics the motion of a ball-and-stick model.

While bending vibrations are responsible for the most pronounced features of the observables shown in Figs. 1 and 2, the experimental data contain more information about the molecular wave packet launched by the pump pulse. One hint of other dynamics is found in the total yield of the (O^+, O^+, S^+) channel, which does not exhibit oscillations at the frequency of the bending vibration. This suggests that double ionization of the cation is insensitive to this mode. However, as depicted in Fig. 3(a), the yield initially decreases by approximately 15% within the first few hundred femtoseconds before flattening out. To explain this behavior, we also plot $\langle\cos^2\theta\rangle$ for this channel in Fig. 3(a). Here, θ is the angle between the laser polarization and $\Delta\vec{p}(O^+) = \vec{p}_1(O^+) - \vec{p}_2(O^+)$, representing the direction of the O-O axis. The strong correlation between these two quantities (except near the overlap region) indicates that the observed yield
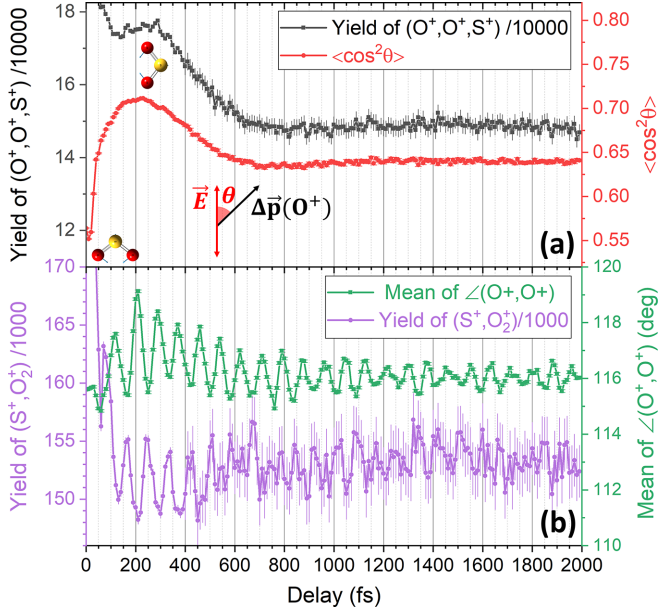
FIG. 3. (a) Delay dependence of the yield (black) and $\langle\cos^2\theta\rangle$ (red) for the (O^+, O^+, S^+) channel, where θ is the angle between the laser polarization and $\Delta\vec{p}(O^+)$. $\Delta\vec{p}(O^+)$ is the vector difference between two O^+ momentum vectors, employed to represent the O-O axis. (b) The average $\angle(O^+, O^+)$ in the (O^+, O^+, S^+) channel (green) and yield of (S^+, O_2^+) channel (purple) as functions of delays. Delays exceeding 400 fs have less statistics, resulting in larger error bars.

FIG. 4. (a), (b) KE sharing between the two O^+ ions for events with delay $\geqslant 200$ fs and large (140°–150°) or small (90°–100°) $\angle(O^+, O^+)$, respectively. (c) Delay-dependent yield of events with a small $\angle(O^+, O^+)$, separated by symmetric and asymmetric KE sharing between the two O^+ ions, defined as $\beta = \Delta KE(O^+, O^+)/KEsum(O^+, O^+)$. Symmetric events have $\beta \leqslant 1/3$, and asymmetric events have $\beta > 1/3$. The separation is represented by the dotted green lines in (a), (b). (d) Distribution of events with small $\angle(O^+, O^+)$ as a function of β following ionization by a single 790 nm or 405 nm laser pulse (obtained via second harmonic generation with a BBO crystal with an estimated intensity and pulse duration of 8×10^{14} W/cm^2 and 30 fs).

variation is due to the initial alignment of the pump-induced rotational wave packet. The time scale is consistent with the rotational dynamics of the two-body breakup channels shown in Fig. S4 (SM) [78]. Although the O-O axis is the most polarizable axis of the molecule, strong-field ionization of neutral SO_2 is more likely to occur along the symmetry axis (see Ref. [61] and SM, Fig. S5 [78]). Thus, SO_2^+ ions are most likely created near the peak of the pump pulse with their symmetry axes aligned with the laser polarization. They then rotate due to the angular momentum accumulated in the pump pulse and reach peak alignment (of the O-O axis) around 200 fs. After the peak, the rotational wave packet dephases and exhibits long-term incoherent alignment.

This rovibrational wave packet motion in SO_2^+ has other manifestations that can be elucidated by multicoincidence momentum imaging. One example is the formation of O_2^+, which can be traced by analyzing the (S^+, O_2^+) coincidence channel. The delay-dependent yield of this channel is shown in Fig. 3(b) along with the mean value of $\angle(O^+, O^+)$ in the three-body channel. Clearly, the two oscillate out of phase, suggesting an intuitive picture of O_2^+ formation by the probe pulse: O_2^+ is more likely to be formed if the probe pulse finds the cation at smaller OSO angles, where the two oxygen atoms are closer to each other. The alignment and bending angle dependence of O_2^+ production may help improve our understanding of a potential source of abiotic oxygen in SO_2-rich planetary atmospheres [65].

The rovibrational wave packet also controls the excitation of the ground-state cations to the first excited state in the probe pulse. This single-photon transition is energetically allowed for $\phi \lesssim 134^\circ$ and its dipole moment is along the O-O axis.
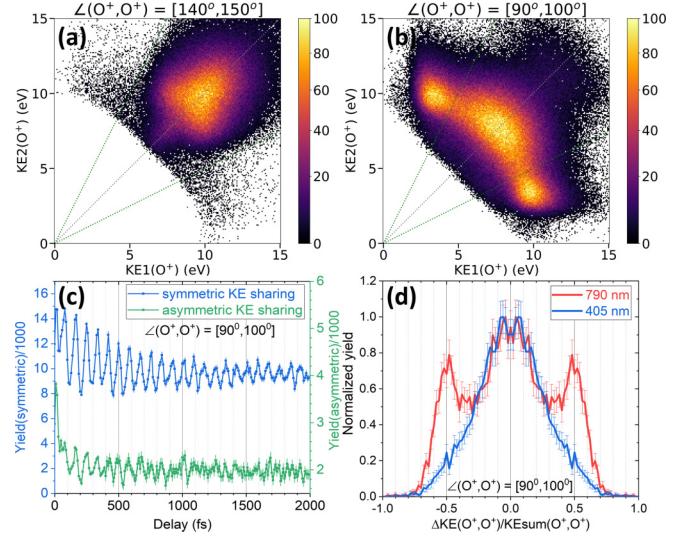
Thus, when ground-state cations have rotated into alignment with the probe laser polarization and bending mode vibration has pushed the nuclear probability density to smaller-than-equilibrium bond angles ($\phi < 134^\circ$), a single photon in the leading edge of the probe can resonantly transfer population from $\tilde{X}^2A_1$ to $\tilde{A}^2B_2$ (Fig. 1). These two states have a symmetry-allowed conical intersection (CI) at $\approx108^\circ$ with the branching space comprised of the bending and asymmetric stretching coordinates [60]. After excitation to $\tilde{A}^2B_2$ the wave packet travels towards the CI where it is nonadiabatically coupled to the asymmetric stretch mode and returns to $\tilde{X}^2A_1$ within 20 fs [60]. Since our probe pulse width is 28 fs, these cations can still be ionized at the peak of the probe and appear in the (O^+, O^+, S^+) channel. On the other hand, if the excitation occurs in the trailing edge of the pump pulse, the wave packet should dephase rapidly as it traverses the CI and not exhibit 400 cm^{-1} oscillations.

In the experimental data, signatures of a wave packet in $\tilde{A}$ are seen in the KE sharing plot for the O^+ ions. We separate events with $\angle(O^+, O^+) \in [140^\circ, 150^\circ]$ and $\angle(O^+, O^+) \in [90^\circ, 100^\circ]$ in Figs. 4(a), 4(b) respectively, with the expectation that the population excited to $\tilde{A}$ can travel to smaller angles than the inner turning point of the bending wave packet in $\tilde{X}$, but not to the outer turning point, within the probe pulse. The strong component with asymmetric KE sharing seen in Fig. 4(b) but not in Fig. 4(a) confirms the dipole coupling to $\tilde{A}$ and nonadiabatic coupling to the asymmetric stretch mode. Figure 4(c) shows the delay-dependent yields

of events with symmetric (blue) and asymmetric (green) KE sharing [all with small $\angle(O^+, O^+)$]. The in-phase oscillation of the two curves is consistent with population transfer by the probe to $\tilde{A}$ near the inner turning point of the ground-state bending vibration. To further test this hypothesis of resonant interstate coupling, we use a single laser pulse at 405 nm to Coulomb explode SO_2 into (O^+, O^+, S^+). At this shorter wavelength, efficient dipole coupling can occur only near the outer turning point of the $\tilde{X}$ wave packet and is unlikely to occur within our 30-fs pulse. The absence of asymmetric KE sharing peaks in the 405-nm case [Fig. 4(d)] confirms a resonant coupling near 790 nm, corroborating our conclusion that we see signatures of mode coupling at the CI in our pump-probe experiment.

In conclusion, our work highlights the direct sensitivity of CEI to changes in the spatial density of the nuclear wave packet propagating on multiple electronic states, demonstrating the feasibility of tracking correlated atomic motion within a molecule. Our multidimensional coincident measurement allows us to observe and interpret the interplay between rotational, vibrational, and electronic motion, which determines the molecular wave-packet evolution and experimental observables. Notably, correlated fragment momenta reveal clear signatures of a conical intersection that couples the bending and asymmetric stretching coordinates, which

is difficult to access with other experimental techniques. This study paves the way for tracking coupled electronic and nuclear dynamics in medium-size polyatomic molecules, where high-order correlations revealed by CEI provide unique insights into the 3D correlated motion of multiple atomic constituents. Recent advancements have shown that CEI can image detailed 3D structures of gas-phase molecules with about ten atoms [25,26,88,89], bringing this goal closer to reality.

[1] A. H. Zewail, Femtochemistry: Atomic-scale dynamics of the chemical bond, J. Phys. Chem. A **104**, 5660 (2000).

[2] A. A. Ischenko, P. M. Weber, and R. J. D. Miller, Capturing chemistry in action with electrons: Realization of atomically resolved reaction dynamics, Chem. Rev. **117**, 11066 (2017).

[3] M. Ivanov, Concluding remarks: The age of molecular movies, Faraday Discuss. **228**, 622 (2021).

[4] M. Zhang, Z. Guo, X. Mi, Z. Li, and Y. Liu, Ultrafast imaging of molecular dynamics using ultrafast low-frequency lasers, x-ray free electron lasers, and electron pulses, J. Phys. Chem. Lett. **13**, 1668 (2022).

[5] S. P. Weathersby, G. Brown, M. Centurion, T. F. Chase, R. Coffee, J. Corbett, J. P. Eichner, J. C. Frisch, A. R. Fry, M. Gühr, N. Hartmann, C. Hast, R. Hettel, R. K. Jobe, E. N. Jongewaard, J. R. Lewandowski, R. K. Li, A. M. Lindenberg, I. Makasyuk, J. E. May, D. McCormick, M. N. Nguyen, A. H. Reid, X. Shen, K. Sokolowski-Tinten, T. Vecchione, S. L. Vetter, J. Wu, J. Yang, H. A. Dürr, and X. J. Wang, Mega-electron-volt ultrafast electron diffraction at SLAC National Accelerator Laboratory, Rev. Sci. Instrum. **86**, 073702 (2015).

[6] D. Filippetto, P. Musumeci, R. K. Li, B. J. Siwick, M. R. Otto, M. Centurion, and J. P. F. Nunes, Ultrafast electron diffraction: Visualizing dynamic states of matter, Rev. Mod. Phys. **94**, 045004 (2022).

[7] M. P. Minitti, J. M. Budarz, A. Kirrander, J. S. Robinson, D. Ratner, T. J. Lane, D. Zhu, J. M. Glownia, M. Kozina, H. T. Lemke, M. Sikorski, Y. Feng, S. Nelson, K. Saita, B. Stankus, T. Northey, J. B. Hastings, and P. M. Weber, Imaging molecular motion: Femtosecond X-Ray scattering of an electrocyclic chemical reaction, Phys. Rev. Lett. **114**, 255501 (2015).

[8] B. Stankus, H. Yong, N. Zotev, J. M. Ruddock, D. Bellshaw, T. J. Lane, M. Liang, S. Boutet, S. Carbajo, J. S. Robinson, W. Du, N. Goff, Y. Chang, J. E. Koglin, M. P. Minitti, A. Kirrander,

and P. M. Weber, Ultrafast X-ray scattering reveals vibrational coherence following Rydberg excitation, Nat. Chem. **11**, 716 (2019).

[9] J. M. Ruddock, H. Yong, B. Stankus, W. Du, N. Goff, Y. Chang, A. Odate, A. M. Carrascosa, D. Bellshaw, N. Zotev, M. Liang, S. Carbajo, J. Koglin, J. S. Robinson, S. Boutet, A. Kirrander, M. P. Minitti, and P. M. Weber, A deep UV trigger for ground-state ring-opening dynamics of 1,3-cyclohexadiene, Sci. Adv. **5**, eaax6625 (2019).

[10] Y. Liu, S. L. Horton, J. Yang, J. P. F. Nunes, X. Shen, T. J. A. Wolf, R. Forbes, C. Cheng, B. Moore, M. Centurion, K. Hegazy, R. Li, M.-F. Lin, A. Stolow, P. Hockett, T. Rozgonyi, P. Marquetand, X. Wang, and T. Weinacht, Spectroscopic and structural probing of excited-state molecular dynamics with time-resolved photoelectron spectroscopy and ultrafast electron diffraction, Phys. Rev. X **10**, 021016 (2020).

[11] D. Polli, P. Altoè, O. Weingart, K. M. Spillane, C. Manzoni, D. Brida, G. Tomasello, G. Orlandi, P. Kukura, R. A. Mathies, M. Garavelli, and G. Cerullo, Conical intersection dynamics of the primary photoisomerization event in vision, Nature (London) **467**, 440 (2010).

[12] H. J. Wörner, J. B. Bertrand, B. Fabre, J. Higuet, H. Ruf, A. Dubrouil, S. Patchkovskii, M. Spanner, Y. Mairesse, V. Blanchet, E. Mével, E. Constant, P. B. Corkum, and D. M. Villeneuve, Conical intersection dynamics in NO_2 probed by homodyne high-harmonic spectroscopy, Science **334**, 208 (2011).

[13] B. G. Levine and T. J. Martínez, Isomerization through conical intersections, Annu. Rev. Phys. Chem. **58**, 613 (2007).

[14] H. Stapelfeldt, E. Constant, and P. B. Corkum, Wave packet structure and dynamics measured by Coulomb explosion, Phys. Rev. Lett. **74**, 3780 (1995).

[15] P. W. Dooley, I. V. Litvinyuk, K. F. Lee, D. M. Rayner, M. Spanner, D. M. Villeneuve, and P. B. Corkum, Direct imaging of rotational wave-packet dynamics of diatomic molecules, Phys. Rev. A **68**, 023406 (2003).

[16] F. Légaré, K. F. Lee, A. D. Bandrauk, D. M. Villeneuve, and P. B. Corkum, Laser Coulomb explosion imaging for probing ultra-fast molecular dynamics, J. Phys. B: At. Mol. Opt. Phys. **39**, S503 (2006).

[17] A. Matsuda, M. Fushitani, E. J. Takahashi, and A. Hishikawa, Visualizing hydrogen atoms migrating in acetylene dication by time-resolved three-body and four-body Coulomb explosion imaging, Phys. Chem. Chem. Phys. **13**, 8697 (2011).

[18] H. Ibrahim, B. Wales, S. Beaulieu, B. E. Schmidt, N. Thiré, E. P. Fowe, É. Bisson, C. T. Hebeisen, V. Wanie, M. Giguére, J.-C. Kieffer, M. Spanner, A. D. Bandrauk, J. Sanderson, M. S. Schuurman, and F. Légaré, Tabletop imaging of structural evolutions in chemical reactions demonstrated for the acetylene cation, Nat. Commun. **5**, 4422 (2014).

[19] E. T. Karamatskos, S. Raabe, T. Mullins, A. Trabattoni, P. Stammer, G. Goldsztejn, R. R. Johansen, K. Długołecki, H. Stapelfeldt, M. J. J. Vrakking, S. Trippel, A. Rouzée, and J. Küpper, Molecular movie of ultrafast coherent rotational dynamics of OCS, Nat. Commun. **10**, 3364 (2019).

[20] X. Yu, X. Zhang, X. Hu, X. Zhao, D. Ren, X. Li, P. Ma, C. Wang, Y. Wu, S. Luo, and D. Ding, Femtosecond time-resolved neighbor roles in the fragmentation dynamics of molecules in a dimer, Phys. Rev. Lett. **129**, 023001 (2022).

[21] J. Ullrich, R. Moshammer, R. Dörner, O. Jagutzki, V. Mergel, H. Schmidt-Böcking, and L. Spielberger, Recoil-ion momentum spectroscopy, J. Phys. B: At. Mol. Opt. Phys. **30**, 2917 (1997).

[22] F. Légaré, K. F. Lee, I. V. Litvinyuk, P. W. Dooley, S. S. Wesolowski, P. R. Bunker, P. Dombi, F. Krausz, A. D. Bandrauk, D. M. Villeneuve, and P. B. Corkum, Laser Coulomb-explosion imaging of small molecules, Phys. Rev. A **71**, 013415 (2005).

[23] A. Rudenko, T. Ergler, B. Feuerstein, K. Zrost, C. D. Schröter, R. Moshammer, and J. Ullrich, Real-time observation of vibrational revival in the fastest molecular system, Chem. Phys. **329**, 193 (2006).

[24] H. Schmidt-Böcking, J. Ullrich, R. Dörner, and C. L. Cocke, The COLTRIMS reaction microscope—the spyhole into the ultrafast entangled dynamics of atomic and molecular systems, Ann. Phys. **533**, 2100134 (2021).

[25] R. Boll, J. M. Schäfer, B. Richard, K. Fehre, G. Kastirke, Z. Jurek, M. S. Schöffler, M. M. Abdullah, N. Anders, T. M. Baumann, S. Eckart, B. Erk, A. D. Fanis, R. Dörner, S. Grundmann, P. Grychtol, A. Hartung, M. Hofmann, M. Ilchen, L. Inhester, C. Janke, R. Jin, M. Kircher, K. Kubicek, M. Kunitski, X. Li, T. Mazza, S. Meister, N. Melzer, J. Montano, V. Music, G. Nalin, Y. Ovcharenko, C. Passow, A. Pier, N. Rennhack, J. Rist, D. E. Rivas, D. Rolles, I. Schlichting, L. P. H. Schmidt, P. Schmidt, J. Siebert, N. Strenger, D. Trabert, F. Trinter, I. Vela-Perez, R. Wagner, P. Walter, M. Weller, P. Ziolkowski, S.-K. Son, A. Rudenko, M. Meyer, R. Santra, and T. Jahnke, X-ray multiphoton-induced Coulomb explosion images complex single molecules, Nat. Phys. **18**, 423 (2022).

[26] H. V. S. Lam, A. S. Venkatachalam, S. Bhattacharyya, K. Chen, K. Borne, E. Wang, R. Boll, T. Jahnke, V. Kumarappan, A. Rudenko, and D. Rolles, Differentiating three-dimensional molecular structures using laser-induced Coulomb explosion imaging, Phys. Rev. Lett. **132**, 123201 (2024).

[27] H. V. S. Lam, A. S. Venkatachalam, S. Bhattacharyya, E. Wang, K. Borne, K. Chen, A. Rudenko, and D. Rolles, Coulomb explosion imaging: A robust method for distinguishing molecular structures and tracking structural changes in photochemical reactions, in *Ultrafast Nonlinear Imaging and Spectroscopy XI*, edited by Z. Liu, D. Psaltis, and K. Shi, International Society for Optics and Photonics, Vol. 12681 (SPIE, Bellingham, 2023), p. 1268108.

[28] T. Endo, S. P. Neville, V. Wanie, S. Beaulieu, C. Qu, J. Deschamps, P. Lassonde, B. E. Schmidt, H. Fujise, M. Fushitani, A. Hishikawa, P. L. Houston, J. M. Bowman, M. S. Schuurman, F. Légaré, and H. Ibrahim, Capturing roaming molecular fragments in real time, Science **370**, 1072 (2020).

[29] F. Rosca-Pruna and M. J. J. Vrakking, Experimental observation of revival structures in picosecond laser-induced alignment of I_2, Phys. Rev. Lett. **87**, 153902 (2001).

[30] K. F. Lee, D. M. Villeneuve, P. B. Corkum, A. Stolow, and J. G. Underwood, Field-free three-dimensional alignment of polyatomic molecules, Phys. Rev. Lett. **97**, 173001 (2006).

[31] J. Yang, M. Guehr, T. Vecchione, M. S. Robinson, R. Li, N. Hartmann, X. Shen, R. Coffee, J. Corbett, A. Fry, K. Gaffney, T. Gorkhover, C. Hast, K. Jobe, I. Makasyuk, A. Reid, J. Robinson, S. Vetter, F. Wang, S. Weathersby, C. Yoneda, M. Centurion, and X. Wang, Diffractive imaging of a rotational wavepacket in nitrogen molecules with femtosecond megaelectronvolt electron pulses, Nat. Commun. **7**, 11232 (2016).

[32] L. Fang and G. N. Gibson, Investigating excited electronic states of I_2^+ and I_2^{2+} produced by strong-field ionization using vibrational wave packets, Phys. Rev. A **75**, 063410 (2007).

[33] J. Yang, M. Guehr, X. Shen, R. Li, T. Vecchione, R. Coffee, J. Corbett, A. Fry, N. Hartmann, C. Hast, K. Hegazy, K. Jobe, I. Makasyuk, J. Robinson, M. S. Robinson, S. Vetter, S. Weathersby, C. Yoneda, X. Wang, and M. Centurion, Diffractive imaging of coherent nuclear motion in isolated molecules, Phys. Rev. Lett. **117**, 153002 (2016).

[34] J. M. Glownia, A. Natan, J. P. Cryan, R. Hartsock, M. Kozina, M. P. Minitti, S. Nelson, J. Robinson, T. Sato, T. van Driel, G. Welch, C. Weninger, D. Zhu, and P. H. Bucksbaum, Self-referenced coherent diffraction X-ray movie of Ångstrom- and femtosecond-scale atomic motion, Phys. Rev. Lett. **117**, 153003 (2016).

[35] P. M. Felker and A. H. Zewail, Dynamics of intramolecular vibrational-energy redistribution (IVR). I. Coherence effects, J. Chem. Phys. **82**, 2961 (1985).

[36] P. M. Felker and A. H. Zewail, Dynamics of intramolecular vibrational-energy redistribution (IVR). III. Role of molecular rotations, J. Chem. Phys. **82**, 2994 (1985).

[37] M. Dantus, R. M. Bowman, and A. H. Zewail, Femtosecond laser observations of molecular vibration and rotation, Nature (London) **343**, 737 (1990).

[38] K. Ohmori, Wave-packet and coherent control dynamics, Annu. Rev. Phys. Chem. **60**, 487 (2009).

[39] B. Zhang, Unraveling vibrational wavepacket dynamics using femtosecond ion yield spectroscopy and photoelectron imaging, Chin. J. Chem. Phys. **32**, 35 (2019).

[40] S. M. Poullain, Y. Kobayashi, K. F. Chang, and S. R. Leone, Visualizing coherent vibrational motion in the molecular iodine

$B\,^3\Pi_{0^+_u}$ state using ultrafast XUV transient-absorption spectroscopy, Phys. Rev. A **104**, 022817 (2021).

[41] S. Karashima, Y.-I. Suzuki, and T. Suzuki, Ultrafast extreme ultraviolet photoelectron spectroscopy of nonadiabatic photodissociation of CS$_2$ from ^{1}B$_2$($^1\Sigma_u^+$) state: Product formation via an intermediate electronic state, J. Phys. Chem. Lett. **12**, 3755 (2021).

[42] P. Rupprecht, L. Aufleger, S. Heinze, A. Magunia, T. Ding, M. Rebholz, S. Amberg, N. Mollov, F. Henrich, M. W. Haverkort, C. Ott, and T. Pfeifer, Resolving vibrations in a polyatomic molecule with femtometer precision via x-ray spectroscopy, Phys. Rev. A **108**, 032816 (2023).

[43] S. Karashima, A. Humeniuk, and T. Suzuki, Vibrational motions in ultrafast electronic relaxation of pyrazine, J. Am. Chem. Soc. **146**, 11067 (2024).

[44] A. S. Alnaser, B. Ulrich, X. M. Tong, I. V. Litvinyuk, C. M. Maharjan, P. Ranitovic, T. Osipov, R. Ali, S. Ghimire, Z. Chang, C. D. Lin, and C. L. Cocke, Simultaneous real-time tracking of wave packets evolving on two different potential curves in H$_2^+$ and D$_2^+$, Phys. Rev. A **72**, 030702(R) (2005).

[45] T. Ergler, A. Rudenko, B. Feuerstein, K. Zrost, C. D. Schröter, R. Moshammer, and J. Ullrich, Spatiotemporal imaging of ultrafast molecular motion: Collapse and revival of the D$_2^+$ nuclear wave packet, Phys. Rev. Lett. **97**, 193001 (2006).

[46] I. A. Bocharova, H. Mashiko, M. Magrakvelidze, D. Ray, P. Ranitovic, C. L. Cocke, and I. V. Litvinyuk, Direct Coulomb-explosion imaging of coherent nuclear dynamics induced by few-cycle laser pulses in light and heavy hydrogen, Phys. Rev. A **77**, 053407 (2008).

[47] I. A. Bocharova, A. S. Alnaser, U. Thumm, T. Niederhausen, D. Ray, C. L. Cocke, and I. V. Litvinyuk, Time-resolved coulomb-explosion imaging of nuclear wave-packet dynamics induced in diatomic molecules by intense few-cycle laser pulses, Phys. Rev. A **83**, 013417 (2011).

[48] S. De, I. A. Bocharova, M. Magrakvelidze, D. Ray, W. Cao, B. Bergues, U. Thumm, M. F. Kling, I. V. Litvinyuk, and C. L. Cocke, Tracking nuclear wave-packet dynamics in molecular oxygen ions with few-cycle infrared laser pulses, Phys. Rev. A **82**, 013408 (2010).

[49] S. De, M. Magrakvelidze, I. A. Bocharova, D. Ray, W. Cao, I. Znakovskaya, H. Li, Z. Wang, G. Laurent, U. Thumm, M. F. Kling, I. V. Litvinyuk, I. Ben-Itzhak, and C. L. Cocke, Following dynamic nuclear wave packets in N$_2$, O$_2$, and CO with few-cycle infrared pulses, Phys. Rev. A **84**, 043410 (2011).

[50] S. Erattupuzha, S. Larimian, A. Baltuška, X. Xie, and M. Kitzler, Two-pulse control over double ionization pathways in CO$_2$, J. Chem. Phys. **144**, 024306 (2016).

[51] A. Rudenko, V. Makhija, A. Vajdi, T. Ergler, M. Schürholz, R. K. Kushawaha, J. Ullrich, R. Moshammer, and V. Kumarappan, Strong-field-induced wave packet dynamics in carbon dioxide molecule, Faraday Discuss. **194**, 463 (2016).

[52] Y. Malakar, W. L. Pearson, M. Zohrabi, B. Kaderiya, K. R. P., F. Ziaee, S. Xue, A. T. Le, I. Ben-Itzhak, D. Rolles, and A. Rudenko, Time-resolved imaging of bound and dissociating nuclear wave packets in strong-field ionized iodomethane, Phys. Chem. Chem. Phys. **21**, 14090 (2019).

[53] C. B. Madsen, L. B. Madsen, S. S. Viftrup, M. P. Johansson, T. B. Poulsen, L. Holmegaard, V. Kumarappan, K. A. Jørgensen, and H. Stapelfeldt, Manipulating the torsion of molecules by strong laser pulses, Phys. Rev. Lett. **102**, 073007 (2009).

[54] L. Christensen, J. H. Nielsen, C. B. Brandt, C. B. Madsen, L. B. Madsen, C. S. Slater, A. Lauer, M. Brouard, M. P. Johansson, B. Shepperson, and H. Stapelfeldt, Dynamic stark control of torsional motion by a pair of laser pulses, Phys. Rev. Lett. **113**, 073005 (2014).

[55] W. W. Watson and A. E. Parker, The ultraviolet absorption spectrum of sulfur dioxide, Phys. Rev. **37**, 1484 (1931).

[56] J. H. Clements, On the absorption spectrum of sulphur dioxide, Phys. Rev. **47**, 224 (1935).

[57] C. Lévêque, A. Komainda, R. Taïeb, and H. Köppel, *Ab initio* quantum study of the photodynamics and absorption spectrum for the coupled 1^1A_2 and 1^1B_1 states of SO$_2$, J. Chem. Phys. **138**, 044320 (2013).

[58] I. Wilkinson, A. E. Boguslavskiy, J. Mikosch, J. B. Bertrand, H. J. Wörner, D. M. Villeneuve, M. Spanner, S. Patchkovskii, and A. Stolow, Excited state dynamics in SO$_2$. I. Bound state relaxation studied by time-resolved photoelectron-photoion coincidence spectroscopy, J. Chem. Phys. **140**, 204301 (2014).

[59] S. Mai, P. Marquetand, and L. González, Non-adiabatic and intersystem crossing dynamics in SO$_2$. II. The role of triplet states in the bound state dynamics studied by surface-hopping simulations, J. Chem. Phys. **140** (2014).

[60] C. Lévêque, H. Köppel, and R. Taïeb, Excited state dynamics in SO$_2$. III. An *ab initio* quantum study of single- and multi-photon ionization, J. Chem. Phys. **140**, 204303 (2014).

[61] L. S. Spector, M. Artamonov, S. Miyabe, T. Martinez, T. Seideman, M. Guehr, and P. H. Bucksbaum, Axis-dependence of molecular high harmonic emission in three dimensions, Nat. Commun. **5**, 3190 (2014).

[62] P. Salén, V. Yatsyna, L. Schio, R. Feifel, M. af Ugglas, R. Richter, M. Alagia, S. Stranges, and V. Zhaunerchyk, Complete dissociation branching fractions and Coulomb explosion dynamics of SO$_2$ induced by excitation of O 1s pre-edge resonances, J. Chem. Phys. **143**, 134302 (2015).

[63] L. Chen, E. Wang, W. Zhao, M. Gong, X. Shan, and X. Chen, Fragmentation of SO$_2^{q+}$($q = 2 - 4$) induced by 1 keV electron collision, J. Chem. Phys. **158**, 054301 (2023).

[64] K. Lin, X. Hu, S. Pan, F. Chen, Q. Ji, W. Zhang, H. Li, J. Qiang, F. Sun, X. Gong, H. Li, P. Lu, J. Wang, Y. Wu, and J. Wu, Femtosecond resolving photodissociation dynamics of the SO$_2$ molecule, J. Phys. Chem. Lett. **11**, 3129 (2020).

[65] M. Wallner, M. Jarraya, E. Olsson, V. Ideböhn, R. J. Squibb, S. B. Yaghlane, G. Nyman, J. H. Eland, R. Feifel, and M. Hochlaf, Abiotic molecular oxygen production—ionic pathway from sulfur dioxide, Sci. Adv. **8**, eabq5411 (2022).

[66] D. Rösch, Y. Xu, H. Guo, X. Hu, and D. L. Osborn, SO$_2$ photodissociation at 193 nm directly forms S(^{3}P) + O$_2$($^3\Sigma_g^-$): Implications for the archean atmosphere on earth, J. Phys. Chem. Lett. **14**, 3084 (2023).

[67] Z. Li, Y.-L. Fu, Z. Luo, S. Yang, Y. Wu, H. Wu, G. Wu, W. Zhang, B. Fu, K. Yuan, D. Zhang, and X. Yang, Roaming in highly excited states: The central atom elimination of triatomic molecule decomposition, Science **383**, 746 (2024).

[68] C. M. Maharjan, Ph.D. dissertation, Kansas State University, 2007.

[69] J. Eland and C. Danby, Photoelectron spectra and ionic structure of carbon dioxide, carbon disulphide and sulphur dioxide, Int. J. Mass Spectrom. Ion Phys. **1**, 111 (1968).

[70] L. Wang, Y. T. Lee, and D. A. Shirley, Molecular beam photoelectron spectroscopy of SO_2: Geometry, spectroscopy, and dynamics of SO_2^+, J. Chem. Phys. **87**, 2489 (1987).

[71] D. Holland, M. MacDonald, M. Hayes, P. Baltzer, L. Karlsson, M. Lundqvist, B. Wannberg, and W. von Niessen, An experimental and theoretical study of the valence shell photoelectron spectrum of sulphur dioxide, Chem. Phys. **188**, 317 (1994).

[72] Y. Mo, J. Yang, and G. Chen, Zero kinetic energy photoelectron study of $SO_2^+(X^2A_1)$ using coherent extreme ultraviolet radiation, J. Chem. Phys. **120**, 1263 (2004).

[73] X. Zhang, H. Zheng, R. Li, J. Liang, and Z. Cui, *Ab initio* calculations and spectral simulation of the photoionization process, J. Mol. Struct (THEOCHEM) **822**, 122 (2007).

[74] S. R. Polo and M. K. Wilson, Infrared spectrum of $S^{16}O^{18}O$ and the potential constants of SO_2, J. Chem. Phys. **22**, 900 (1954).

[75] E. Goll, G. Wunner, and A. Saenz, Formation of ground-state vibrational wave packets in intense ultrashort laser pulses, Phys. Rev. Lett. **97**, 103003 (2006).

[76] L. Fang and G. N. Gibson, Strong-field induced vibrational coherence in the ground electronic state of hot I_2, Phys. Rev. Lett. **100**, 103003 (2008).

[77] Z. Wei, J. Li, L. Wang, S. T. See, M. H. Jhon, Y. Zhang, F. Shi, M. Yang, and Z.-H. Loh, Elucidating the origins of multimode vibrational coherences of polyatomic molecules induced by intense laser fields, Nat. Commun. **8**, 735 (2017).

[78] See Supplemental Material at http://link.aps.org/supplemental/10.1103/1yd8-786g for additional data and analyses, including molecular movies that illustrate the correlated motion of individual atoms within the molecule in ion-momentum space.

[79] A. Matsuda, E. J. Takahashi, and A. Hishikawa, Time-resolved laser Coulomb explosion imaging using few-cycle intense laser pulses: Application to exploding CS_2 in highly charged states, J. Electron Spectrosc. Relat. Phenom. **195**, 327 (2014).

[80] H. V. S. Lam, Ph.D. dissertation, Kansas State University, 2021.

[81] V. Makhija, X. Ren, D. Gockel, A.-T. Le, and V. Kumarappan, Orientation resolution through rotational coherence spectroscopy, arXiv:1611.06476.

[82] H. V. S. Lam, S. Yarlagadda, A. Venkatachalam, T. N. Wangjam, R. K. Kushawaha, C. Cheng, P. Svihra, A. Nomerotski, T. Weinacht, D. Rolles, and V. Kumarappan, Angle-dependent strong-field ionization and fragmentation of carbon dioxide measured using rotational wave packets, Phys. Rev. A **102**, 043119 (2020).

[83] T. N. Wangjam, H. V. S. Lam, and V. Kumarappan, Strong-field ionization of the triplet ground state of O_2, Phys. Rev. A **104**, 043112 (2021).

[84] H. V. S. Lam, T. N. Wangjam, and V. Kumarappan, Alignment dependence of photoelectron angular distributions in the few-photon ionization of molecules by ultraviolet pulses, Phys. Rev. A **105**, 053109 (2022).

[85] V.-H. Hoang and U. Thumm, Dissociative ionization of CO_2 in XUV pump and IR or visible probe pulses, Phys. Rev. A **109**, 033117 (2024).

[86] G. M. J. Barca *et al.*, Recent developments in the general atomic and molecular electronic structure system, J. Chem. Phys. **152**, 154102 (2020).

[87] M. Magrakvelidze, A. Kramer, K. Bartschat, and U. Thumm, Complementary imaging of the nuclear dynamics in laser-excited diatomic molecular ions in the time and frequency domains, J. Phys. B: At. Mol. Opt. Phys. **47**, 124003 (2014).

[88] E. Wang, S. Bhattacharyya, K. Chen, K. Borne, F. Ziaee, S. Pathak, H. V. S. Lam, A. S. Venkatachalam, X. Chen, R. Boll, T. Jahnke, A. Rudenko, and D. Rolles, Time-resolved Coulomb explosion imaging unveils ultrafast ring opening of Furan, arXiv:2311.05099.

[89] T. Jahnke, S. Mai, S. Bhattacharyya, K. Chen, R. Boll, M. E. Castellani, S. Dold, U. Frühling, A. E. Green, M. Ilchen, R. Ingle, G. Kastirke, H. V. S. Lam, F. Lever, D. Mayer, T. Mazza, T. Mullins, Y. Ovcharenko, B. Senftleben, F. Trinter, Atia-Tul-Noor, S. Usenko, A. S. Venkatachalam, A. Rudenko, D. Rolles, M. Meyer, H. Ibrahim, and M. Gühr, Direct observation of ultrafast symmetry reduction during internal conversion of 2-thiouracil using Coulomb explosion imaging, Nat. Commun. **16**, 2074 (2025).

Supplemental Material for
Imaging coupled vibrational, rotational, and electronic wave packet dynamics in a triatomic molecule

Huynh Van Sa Lam,[1, *] Van-Hung Hoang,[1] Anbu Selvam Venkatachalam,[1] Surjendu Bhattacharyya,[1] Keyu Chen,[1] Sina Jacob,[2] Sanduni Kudagama,[1] Tu Thanh Nguyen,[1] Daniel Rolles,[1] Uwe Thumm,[1] Artem Rudenko,[1, †] and Vinod Kumarappan[1, ‡]

[1]*James R. Macdonald Laboratory, Kansas State University, Manhattan, KS 66506, USA*
[2]*Institut für Kernphysik, Goethe-Universität Frankfurt, 60438 Frankfurt am Main, Germany*
(Dated: March 5, 2025)

In this Supplemental Material, we provide information that is useful to a subset of readers (who are interested in more specialized content) but is not essential to comprehend the main results of the article. The Supplemental Material includes the following figures: Original data before subtraction, additional results on rotation, simulation showing correlations between observables as a function of the bond angle, and experimental data depicting angle-dependent strong-field ionization rate from SO_2 to SO_2^+ by a linearly polarized intense laser pulse. We also provide the molecular movies (timed sequence of momentum images) as media files, illustrating the correlated motion of individual atoms within the molecule in ion-momentum space.

List of figures and movies:
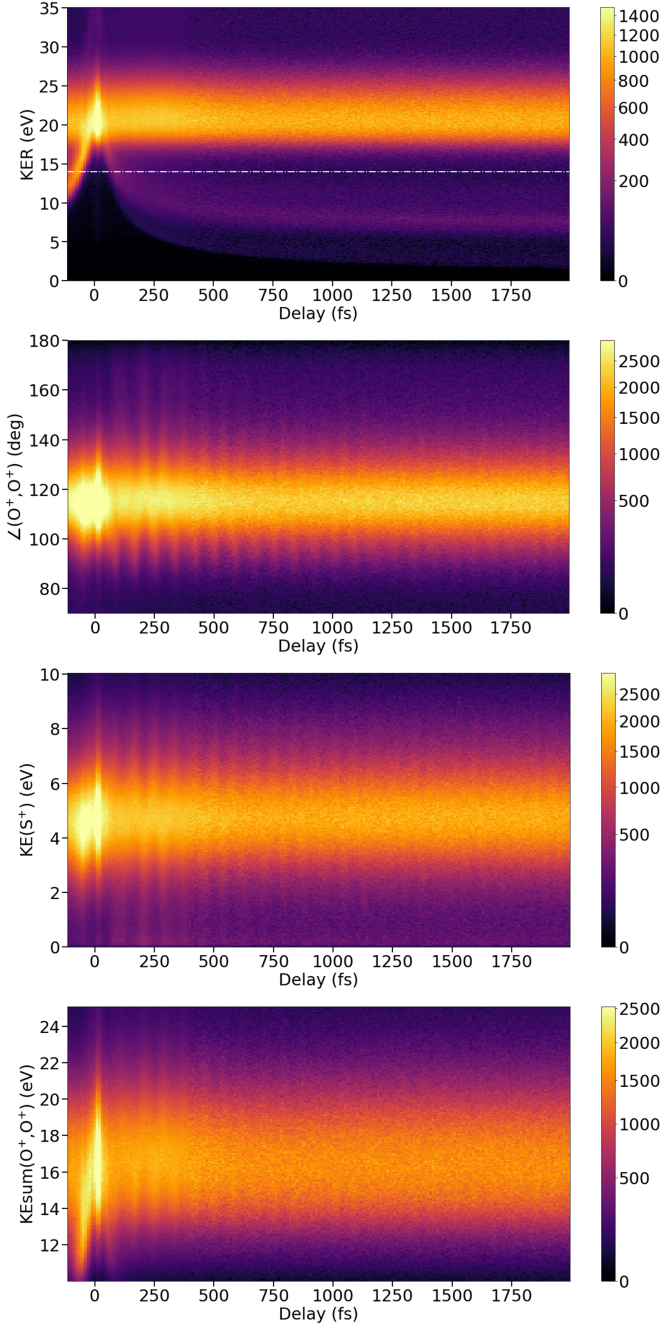
---

* Email: huynhlam@ksu.edu
† Email: rudenko@ksu.edu
‡ Email: vinod@phys.ksu.edu

FIG. S1. Original data before subtraction. From top to bottom: total kinetic energy release (KER), $\angle(O^+, O^+)$, $KE(S^+)$, and $KEsum(O^+, O^+)$. The horizontal dashed line in the KER spectrum is at $14\,eV$. In the main paper, we analyze events with $KER > 14\,eV$. It is worth noting that since $KE(S^+)$ and $KEsum(O^+, O^+)$ are out of phase, the total kinetic energy release (KER, which is the sum of these two) does not oscillate as a function of delay. The total yield of the three-body coincidence channel also remains relatively flat. These two observables do not show the signature of bending vibration.
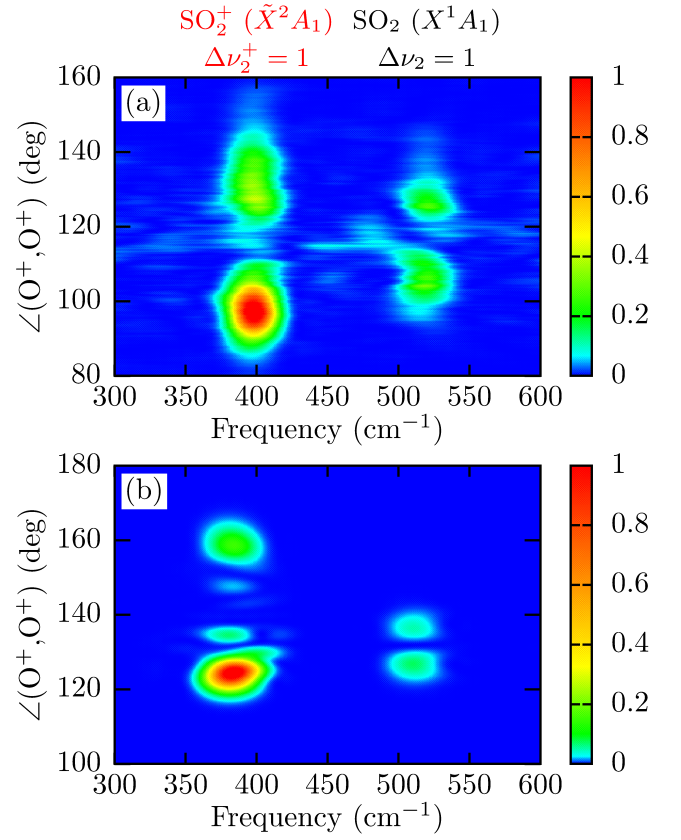

FIG. S2. FFT spectra as a function of $\angle(O^+, O^+)$ from experimental data (top) and theoretical simulation (bottom). Although clearly dominated by the ionic ground-state vibrations, the FFT spectra also manifest a weaker but clear signature of the ground-state bending vibrations in the neutral SO_2 molecule.
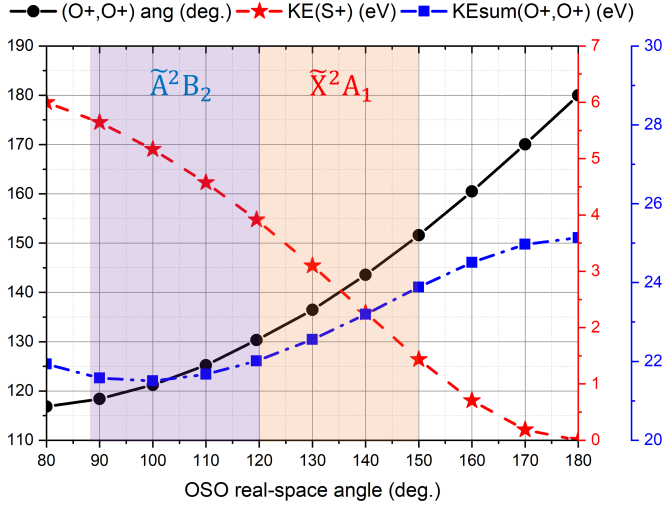
FIG. S3. Simulation showing the dependence of the $\angle(O^+, O^+)$, $KE(S^+)$, and $KEsum(O^+, O^+)$ as a function of the real-space OSO bond angle. The shaded area indicates the expected ranges of the OSO bond angle during the bending motion on the ground and the first excited states of SO_2^+ with classical boundaries following vertical ionization from the ground state of SO_2. In this region, there is a clear correlation between observables: $KE(S^+)$ decreases while $KEsum(O^+, O^+)$ and $\angle(O^+, O^+)$ increases monotonically with larger OSO bond angle. The $\angle(O^+, O^+)$ manifests the same behavior as the OSO bond angle of the nuclear wave packet propagating in the ionic ground state, giving an intuitive picture of the nuclear motion. In this simulation, the potential of the final charge state is assumed to be Coulombic potential, where each atom has a $+1$ point charge.
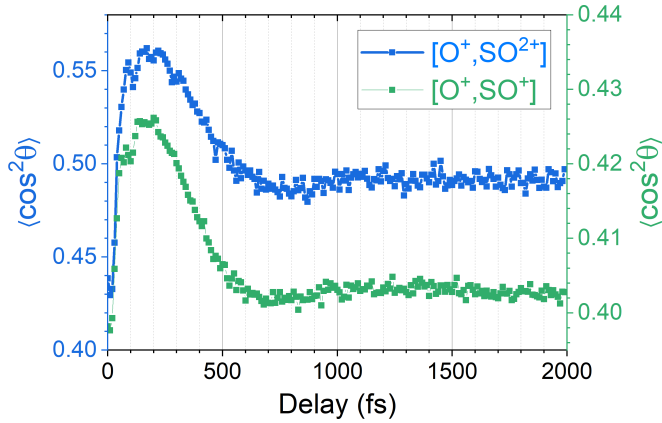

FIG. S4. Delay dependence of $\langle \cos^2 \theta \rangle$, where θ is the angle between the laser polarization and the recoil axis for two-body coincidence channels: (O^+, SO^{2+}) (blue) and (O^+, SO^+) (green). The extracted rotation time scale is consistent with the time scale deduced from the three-body (O^+, O^+, S^+) coincidence channel shown in the main paper.
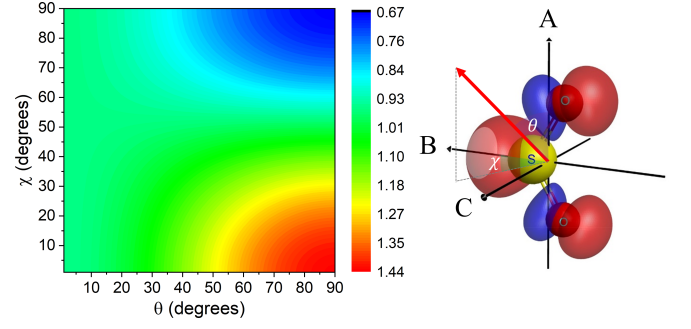

FIG. S5. *Left panel*: Experimentally determined angle-dependent strong-field ionization rate from SO_2 to SO_2^+ by a linearly polarized pulse (adapted from Ref. [1], Sec. 4.2). This result is derived from the delay-dependent yield of SO_2^+ in a pump-probe experiment, where the pump pulse aligns the neutral molecules and the probe pulse ionizes them, using the ORRCS algorithm developed in [2–5]. *Right panel*: Density profile of the highest occupied molecular orbital (HOMO). In the molecular frame, the laser polarization is described by the Euler angles θ and χ, where θ is the polar angle (with the A axis), and χ is the azimuthal angle (on the BC plane). The ionization rate is highest along the B axis ($\theta = 90°, \chi = 0°$) and lowest along the C axis ($\theta = 90°, \chi = 90°$). The angles range from $0°$ to $90°$ because the molecules are aligned but not oriented. In other words, we cannot tell the difference between molecules that rotate $180°$ about the principal axes.
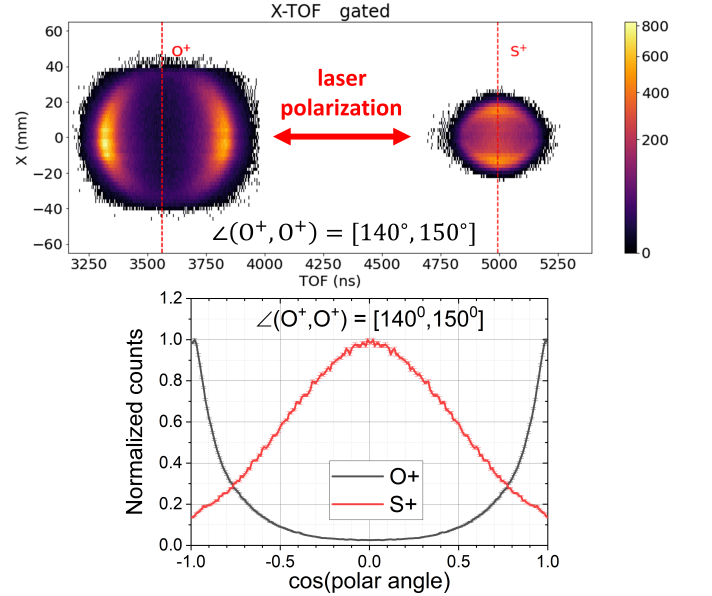

FIG. S6. *Top panel*: Position versus time-of-flight (TOF) spectrum. Only events with large $\angle(O^+, O^+)$, from $140°$ to $150°$, were selected. Most of these events are excited by the pump to $SO_2^+(X^2A_1)$ state before being fragmented into the triply charged channel by the probe. The O^+ fragments have denser distribution along the laser polarization axis, while the S^+ fragment distributes more perpendicular to this axis, suggesting that the probe preferentially ionizes aligned molecules to (O^+, O^+, S^+) channel. *Bottom panel*: Polar angle distributions of O^+ and S^+ in the laboratory frame. On the x axis, 0 means perpendicular to the laser polarization, while -1 and $+1$ mean along the laser polarization.

[1] H. V. S. Lam, *Molecular-frame measurements of light-induced processes using rotational coherences driven by ultrafast laser pulses*, Ph.D. dissertation, Kansas State University, Manhattan, KS (2021), available at https://hdl.handle.net/2097/41566.

[2] V. Makhija, X. Ren, D. Gockel, A.-T. Le, and V. Kumarappan, Orientation Resolution through Rotational Coherence Spectroscopy (2016), arXiv:1611.06476 [physics].

[3] H. V. S. Lam, S. Yarlagadda, A. Venkatachalam, T. N. Wangjam, R. K. Kushawaha, C. Cheng, P. Svihra, A. Nomerotski, T. Weinacht, D. Rolles, and V. Kumarap-pan, Angle-dependent strong-field ionization and fragmentation of carbon dioxide measured using rotational wave packets, Phys. Rev. A **102**, 043119 (2020).

[4] T. N. Wangjam, H. V. S. Lam, and V. Kumarappan, Strong-field ionization of the triplet ground state of O_2, Phys. Rev. A **104**, 043112 (2021).

[5] H. V. S. Lam, T. N. Wangjam, and V. Kumarappan, Alignment dependence of photoelectron angular distributions in the few-photon ionization of molecules by ultraviolet pulses, Phys. Rev. A **105**, 053109 (2022).